



ELSEVIER

Available online at www.sciencedirect.com

SCIENCE @ DIRECT®

Electronic Notes in Discrete Mathematics 20 (2005) 519–534

Electronic Notes in
DISCRETE
MATHEMATICS

www.elsevier.com/locate/ndm

Reconstruction of factor structures using discrete tomography method¹

Antal Nagy^{a,2}, Attila Kuba^{a,3}, and Martin Samal^{b,4}

^a *Department of Image Processing and Computer Graphics, University of Szeged
Szeged, Hungary*

^b *Department of Nuclear Medicine, Charles University Prague
Prague, Czech Republic*

Abstract

Our aim was to estimate the volumes of homogeneous structures whose contrast / intensity was changing with time, using only few (here 4) projections of the structures. Each projection was recorded over a period of time and consisted of a sequence of images. The projections of the structures were first separated by factor analysis of the total projections. Then each structure was reconstructed individually from its factor projections using discrete tomography. Assumed application is the single-photon emission computed tomography (SPECT).

Keywords: Factor analysis, discrete tomography, simulated annealing, dynamic SPECT.

¹ This work has been supported by the OTKA grant T 048476 and NSF grant DMS 0306215

² Email: nagya@inf.u-szeged.hu

³ Email: kuba@inf.u-szeged.hu

⁴ Email: samal@cesnet.cz

1 Introduction

First, we consider the following problem. Let us suppose that there is a 3D dynamic object, which can be represented by a non-negative function $f(r, t)$, where r and t denote the position in space and time, respectively. Suppose that f can be expressed as a linear combination of (so far unknown) binary valued functions $f_k(r)$, $k = 1, 2, \dots, K$ ($K \geq 1$), being constant in time, such that

$$(1) \quad f(r, t) = c_1(t) \cdot f_1(r) + c_2(t) \cdot f_2(r) + \dots + c_K(t) \cdot f_K(r) + \eta(r, t),$$

where $c_k(t)$ denote the k -th weighting coefficient, which depends on time, and $\eta(r, t)$ represents the noise or residual in (r, t) . Given the assumption that η and f are uncorrelated, $c_k(t)$ and $f_k(r)$ are to be determined such that f_i are independent of f_j for all $i \neq j$. If the values of $f(r, t)$ are available then the problem can be solved by factor analysis.

However in some applications, we cannot measure the function f in the points of the space, but we can measure its projections only. This is frequently the case, for example, in nuclear medicine, where the object is the radioactivity distribution in an organ and the projections are gamma camera images from different directions. In such a case, SPECT imaging is applied to collect data for the reconstruction of tomographic slices of the object.

So, we have also a second, a reconstruction problem. In this reconstruction problem we deal with a special *emission tomography* model, where the object to be reconstructed is considered as a set of points emitting rays into all directions of the space, and the space is filled with some material attenuating the rays. It is important that the absorption is included into the definition of projection.

Let $f(r, t)$ denote the intensity function of the object to be reconstructed. Suppose that the absorption in the space is constant and the absorption coefficient is $\mu \geq 0$ everywhere. The half-lines in the space can be described as $l(S, v) = \{S + u \cdot v \mid u \geq 0\}$, where S and v are the start point and the direction of the half-line, respectively. Then the *absorbed projection* of f along $l(S, v)$ in time t can be defined as

$$(2) \quad [\mathcal{P}^{(\mu)} f](S, v, t) = \int_0^{\infty} f(S + u \cdot v, t) \cdot e^{-\mu u} du .$$

Usually, the absorbed projection values are measured along many parallel half-

lines in the same time (e.g., by using line or plane detectors). In such a case we can speak about (absorbed) projections taken in direction v . Our problem is to reconstruct f from *absorbed projections* taken from a few directions, especially if we have only four directions. For the sake of simplicity, let us suppose that the four directions are the opposite horizontal and vertical directions. (In the emission tomography model, opposite projections are not identical because of attenuation.) That is, the given 4 projections are taken from the left, the right, the up, and the down directions. Furthermore, let us suppose that the support of f is the unit cube in any time t (see Fig. 1).

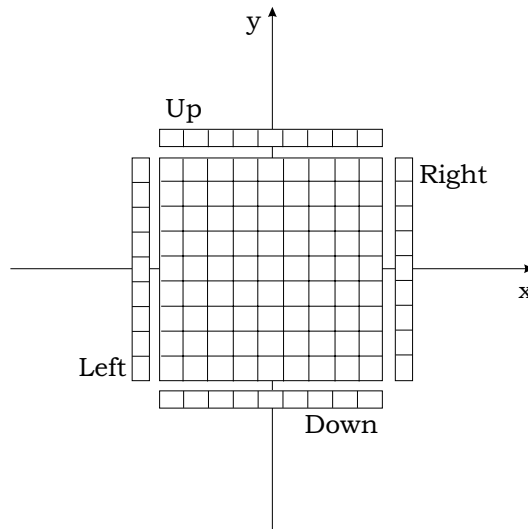


Fig. 1. The arrangement of the 4 absorbed projections illustrated with a square as a 2D section of the unit cube and with 4 lines as the corresponding 4 rows of the 2D projections.

Formally, the *left*, the *right*, the *up*, and the *down absorbed projections* are defined, respectively, as

$$\begin{aligned}
 (3) \quad [\mathcal{L}^{(\mu)} f](y, z, t) &= [\mathcal{P}^{(\mu)} f]((0, y, z), (1, 0, 0), t) \\
 &= \int_0^1 f(u, y, z, t) \cdot e^{-\mu u} du ,
 \end{aligned}$$

$$\begin{aligned}
 (4) \quad [\mathcal{R}^{(\mu)} f](y, z, t) &= [\mathcal{P}^{(\mu)} f]((1, y, z), (-1, 0, 0), t) \\
 &= \int_0^1 f(1 - u, y, z, t) \cdot e^{-\mu u} du ,
 \end{aligned}$$

$$\begin{aligned}
 (5) \quad [\mathcal{U}^{(\mu)} f](x, z, t) &= [\mathcal{P}^{(\mu)} f]((x, 1, z), (0, -1, z), t) \\
 &= \int_0^1 f(x, 1 - u, z, t) \cdot e^{-\mu u} du ,
 \end{aligned}$$

$$\begin{aligned}
 (6) \quad [\mathcal{D}^{(\mu)} f](x, z, t) &= [\mathcal{P}^{(\mu)} f]((x, 0, z), (0, 1, z), t) \\
 &= \int_0^1 f(x, u, z, t) \cdot e^{-\mu u} du .
 \end{aligned}$$

In another words, the equations in (3)-(6) express that the detectors sit on left, right, up, and down sides of the cube look at the cube, and measure the absorbed projections along half lines, which are perpendicular to the corresponding side of the cube.

Summarizing the problem, our task can be divided into two parts. First we have to separate projections of the individual structures from the original projections of the 3D dynamic objects. Afterwards we have to reconstruct the 2D slices of each factor structure from its 4 projections slice by slice. We can repeat this reconstruction for all slices obtaining 3D reconstruction.

The paper consists of the following parts. In Section 2 our phantom model and its implementation are introduced. Afterwards, we describe the details of the applied methods for factor analysis and reconstruction. The results of our experiments together with the related discussion are given in Section 5. Finally, in the last section, we present our conclusions based on the experiences and make suggestions for future work.

2 Phantom

Our phantom (i.e., the function f in (1)) was a simplified 3D mathematical model of the human renal system (it was provided by Dr. W. Backfrieder, AKH Vienna, Austria [1]). The system consists of 5 factors (i.e., $K = 5$), denoted by f_1, f_2, \dots, f_5 in (1), representing two vascular structures, two renal

Table 1
Structures of the given phantom

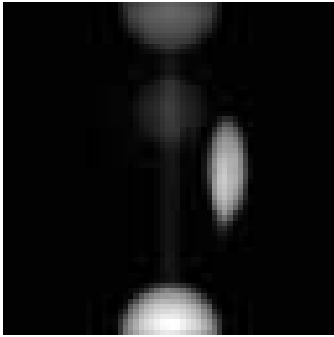
Structure name	Volume (voxels)
Heart and aorta	2652
Liver and spleen	10603
Two renal parenchymas	1350
Two renal pelvises	606
Urinary bladder	2094
Background	rest of the 64^3

structures, and the urinary bladder. Each factor structure is homogeneous, i.e., it is composed of voxels having the same intensity value and its shape is defined by geometric objects (e.g., by discrete spheres and tubes). The factor structures are in a discrete space of 64^3 voxels (the voxel size is $6 \times 6 \times 6$ mm). The background, $\eta(r, t)$ in (1), represents the rest of the cube of the 64^3 voxels. Table 1 gives information about the structures.

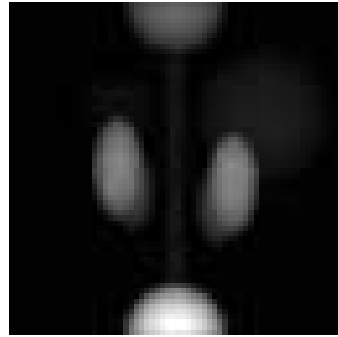
In order to approximate the images of a nuclear medicine SPECT study, absorption, scatter, depth dependent resolution, partial volume effects, and also Poisson noise have been taken into account in the simulation of the projection images. In the model the weights of the factors (i.e., their intensities) change with time according to given functions $c_k(t)$, $k = 1, 2, \dots, 5$, simulating the functionality of the corresponding organs. The four absorbed projections ($\mathcal{L}^{(\mu)}f$, $\mathcal{R}^{(\mu)}f$, $\mathcal{U}^{(\mu)}f$, and $\mathcal{D}^{(\mu)}f$) with size 64×64 each were taken at 120 discrete time moments. The total summation images of the 120 projections for each direction are shown on Fig. 2.

3 Factor analysis

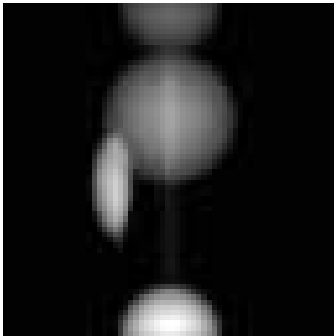
Each simulated factor structure of the whole 3D object had specific dynamics (radioactivity changes with time) according to (1), so, their projections seemed to be separable from the projections of other structures by factor analysis. The factor analysis was performed on each sequence of projections by the method published in [6,7] using spatial constraints. Its results were 20 (i.e., 4×5) 64×64 matrices, denoted by L_k, R_k, U_k , and D_k , $k = 1, 2, \dots, 5$, and the corresponding weighting coefficients $c_k^{(l)}(t)$, $c_k^{(r)}(t)$, $c_k^{(u)}(t)$, and $c_k^{(d)}(t)$ for $k = 1, 2, \dots, 5$.



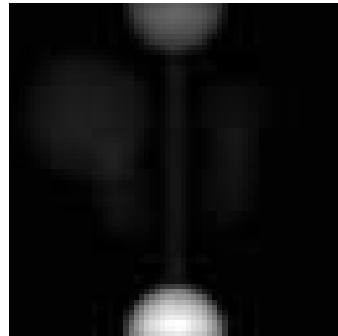
(a) Summation images of the left projections



(b) Summation images of the up projections



(c) Summation images of the right projections

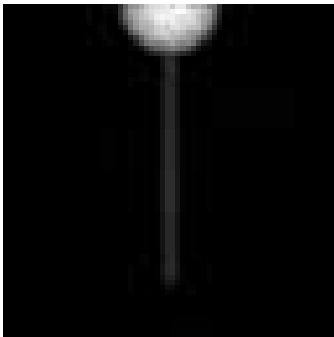


(d) Summation images of the down projections

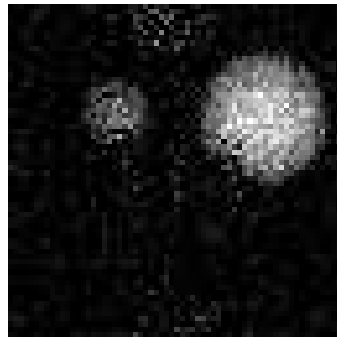
Fig. 2. Summation images of the 120 projections taken from 4 directions.

As examples, the separated 5 images from direction “up”, i.e., the images U_k , $k = 1, 2, \dots, 5$, are shown in Fig. 3. The 20 curves describing the change of the weighting coefficient in time, i.e., $c_k^{(l)}(t)$, $c_k^{(r)}(t)$, $c_k^{(u)}(t)$, and $c_k^{(d)}(t)$ for $k = 1, 2, \dots, 5$ are given in Fig. 4.

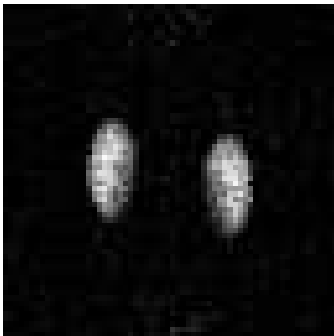
The images and coefficients created by the factor analysis have the follow-



(a) Heart and aorta



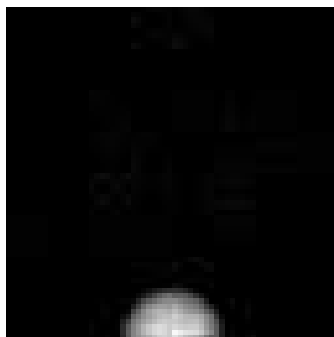
(b) Liver and spleen



(c) Renal parenchymas

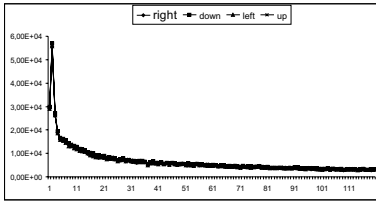


(d) Renal pelvises

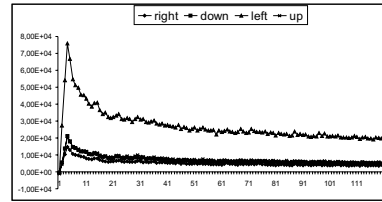


(e) Bladder

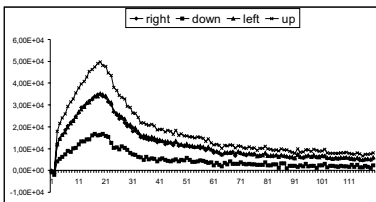
Fig. 3. The images U_k , $k = 1, 2, \dots, 5$, as they are created from the “Up” projections $\mathcal{U}^{(\mu)} f_k$ by factor analysis.



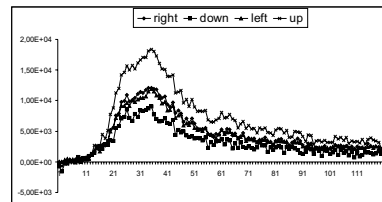
(a) Heart and aorta



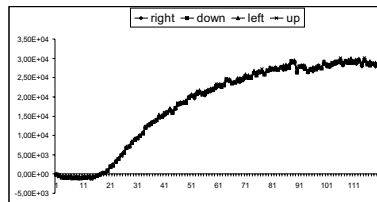
(b) Liver and spleen



(c) Renal parenchymas



(d) Renal pelvises



(e) Bladder

Fig. 4. The curves of the weighting coefficients created by factor analysis. ing relations with the projections of the whole structure.

$$\begin{aligned}
 [\mathcal{L}^{(\mu)} f](y, z, t) &= \sum_{k=1}^5 c_k^{(l)}(t) \cdot L_k(y, z) + \eta_L(y, z, t), \\
 [\mathcal{R}^{(\mu)} f](y, z, t) &= \sum_{k=1}^5 c_k^{(r)}(t) \cdot R_k(y, z) + \eta_R(y, z, t), \\
 [\mathcal{U}^{(\mu)} f](x, z, t) &= \sum_{k=1}^5 c_k^{(u)}(t) \cdot U_k(x, z) + \eta_U(x, z, t), \\
 [\mathcal{D}^{(\mu)} f](x, z, t) &= \sum_{k=1}^5 c_k^{(d)}(t) \cdot D_k(x, z) + \eta_D(x, z, t),
 \end{aligned}$$

where η_L, η_R, η_U , and η_D denote the correspondent residuals. This notation indicates that we could not compute the projections of the factors exactly. However, it is true that

$$(7) \quad \begin{aligned} c_k(t) \cdot [\mathcal{L}^{(\mu)} f_k](y, z) &= c_k^{(l)}(t) \cdot L_k(y, z) , \\ c_k(t) \cdot [\mathcal{R}^{(\mu)} f_k](y, z) &= c_k^{(r)}(t) \cdot R_k(y, z) , \\ c_k(t) \cdot [\mathcal{U}^{(\mu)} f_k](x, z) &= c_k^{(u)}(t) \cdot U_k(x, z) , \\ c_k(t) \cdot [\mathcal{D}^{(\mu)} f_k](x, z) &= c_k^{(d)}(t) \cdot D_k(x, z) , \end{aligned}$$

for all $k = 1, 2, \dots, 5$. That is, the factor analysis could determine the projections of the factors up to a multiplicative constant only.

4 Reconstruction

The equation system (7) shows that the images L_k, R_k, U_k , and D_k cannot be considered as the absorbed projections of the factor f_k , $k = 1, 2, \dots, 5$. However, the absorbed projections of the factor structures can be computed from these images by suitable multiplications. Therefore, before using any kind of reconstruction method, we need determine the multiplicative constants $d_k^{(l)} = c_k^{(l)}(t)/c_k(t)$, $d_k^{(r)} = c_k^{(r)}(t)/c_k(t)$, $d_k^{(u)} = c_k^{(u)}(t)/c_k(t)$, and $d_k^{(d)} = c_k^{(d)}(t)/c_k(t)$, for $k = 1, 2, \dots, 5$. Unfortunately, $c_k(t)$ is not known, so we cannot use these relations for the determination of $d_k^{(l)}$, $d_k^{(r)}$, $d_k^{(u)}$, and $d_k^{(d)}$, for $k = 1, 2, \dots, 5$.

We used another method to get the absorbed projections of the factor structures. The idea is roughly the following (a more detailed description is given in Subsection 4.2). This method, first, reconstructs a representative section of the 3D factor structure trying several multiplicative constants. Then it selects the constants giving the best reconstruction, and, finally, it applies the selected constants as the multiplicative values for the correction of the projections for all sections.

4.1 Reconstruction of a binary matrix from its absorbed projections

Let us suppose that the section of f_k at height $z = z_0$ is to be reconstructed. The section $f_k(x, y, z = z_0)$ can be represented by a binary valued matrix or, equivalently, by a vector $\xi \in \{0, 1\}^J$ where ξ_j denotes the j th element of the matrix $f_k(x, y, z = z_0)$, say, in a row by row order, $j = 0, 1, \dots, J$ and $J = n^2$.

Knowing the four absorbed projections of each f_k we can try to reconstruct them by *emission discrete tomography*, shortly EDT, method [3]. The EDT

reconstruction problem can be described as a linear equation system

$$(8) \quad A\xi = b ,$$

where $b = (b_i)$, $i = 1, 2, \dots, I$, denotes the vector of absorbed projection values and $A = (a_{ij})_{I \times J}$ is the matrix describing the relation between ξ and b . The elements of A can be computed from the geometry of the projections and from the known absorption value μ . Vector b is given by the measurements. We are looking for a binary valued ξ satisfying (8).

Because of noise, measurement errors, and model simplifications we cannot hope to find a ξ satisfying (8) exactly. However, (8) can be reformulated as an optimization problem. Formally, find the minimum of the objective function

$$(9) \quad C(\xi) = \|A\xi - b\| + \gamma \cdot \Phi(\xi) \quad \text{such that } \xi \text{ is binary .}$$

The first term in (9) controls that we have a ξ satisfying (8) at least approximately. The second term gives us the possibility to include *a priori* knowledge about ξ into the optimization if there are several good binary vector candidates for keeping $\|A\xi - b\|$ small. In our experiments we have used the function

$$(10) \quad \Phi(x) = \sum_{j=0}^J \sum_{l \in Q_j^m} g_{l,j} \cdot |\xi_j - \xi_l| ,$$

where Q_j^m is the set of the indexes of the $m \times m$ adjacent pixels of the j th lattice pixel and $g_{l,j}$ is the corresponding element of a matrix representing a 2D $m \times m$ Gaussian matrix. The $g_{l,j}$ scalar weights the differences according to the distance of the two adjacent, l th and j th pixels. Using this regularization term we can force the optimization algorithm to find binary matrices with possibly compact regions of 0s and 1s.

For solving (9) the *simulated annealing* (SA) optimization method [4] was used. The implementation of this algorithm is given in [5].

4.2 Determination of the multiplicative constants

As representative section we selected those which had the highest absorbed projections value. Then a sequence of reconstructions was performed with different constants. From the different reconstruction results the ξ giving the best objective function $C(\xi)$ was selected. The multiplicative constants belonging to the optimal reconstruction of the representative section were used then for all sections.

Table 2
 Statistical results about the reconstructed structures

Structure name	Original volume (voxels)	Reconstructed volume (voxels)	Standard deviation (voxels)
Heart and aorta	2652	2541 (96 %)	5.29
Liver and spleen	10603	9486 (89 %)	100
Renal parenchymas	1350	1450 (107 %)	17.1
Renal pelvises	606	511 (84 %)	5.4
Urinary bladder	2094	1925 (92 %)	3.95

5 Results

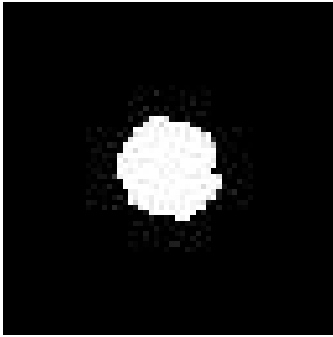
During the reconstruction we had to choose a proper size m for the neighborhood Q_j^m in (10) and suitable value of γ in (9). Setting up all the necessary values, we selected the representative sections for each structure and found the optimal reconstruction. The reconstructed representative slices are given in Fig. 5. For visualization of the reconstructed 3D factor structures we used the software Slicer [8]. The results can be seen in Fig. 6.

The reconstruction method is probabilistic and in this way the results can be different if we repeat the procedure even with the same input data. In order to get information about the differences between the results reconstructed by multiple performances, we repeated the whole process 100 times for each structure. The average volumes were calculated from the repeated reconstruction results, see Table 2. In this table the reconstructed volumes are expressed also as the percentage of the original volumes (see the numbers in brackets). The last column shows the standard deviation of the volumes after repeating the reconstruction 100 times.

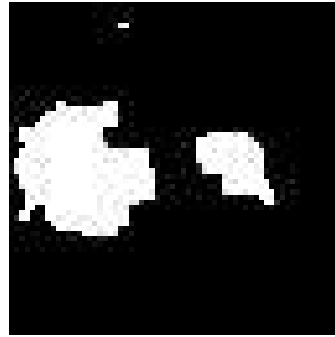
The average slices coming from the repeated reconstruction also have been visualized by Slicer using threshold values for each structure (see. Fig. 8).

6 Discussion and conclusion

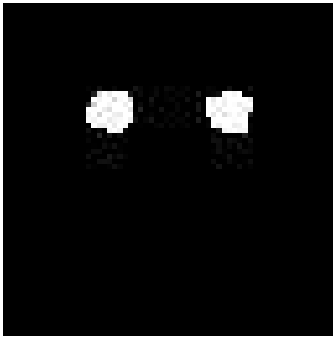
A possible application of DT in SPECT is presented. A two step procedure is suggested to reconstruct 3D factor structures from 4 absorbed projections acquired during a dynamic renal SPECT study. In the first step factor analysis



(a) Heart and aorta, Slice 2



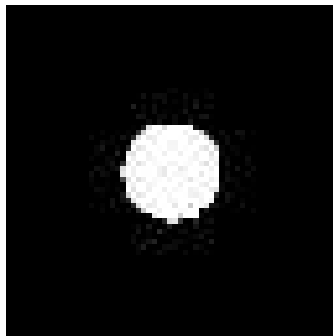
(b) Liver and spleen, Slice 19



(c) Renal parenchymas, Slice 30



(d) Renal pelvises, Slice 39



(e) Bladder, Slice 61

Fig. 5. Representative slices reconstructed by the optimal multiplicative constant settings.

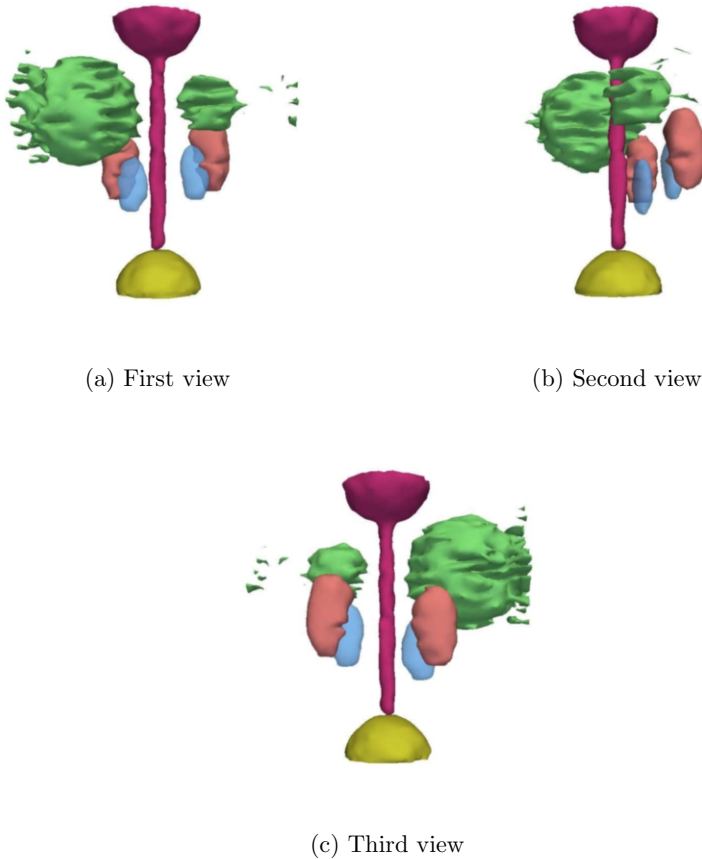
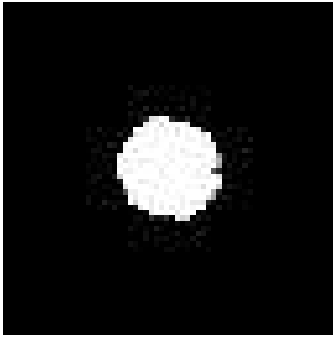


Fig. 6. 3D visualization of the reconstructed structures.

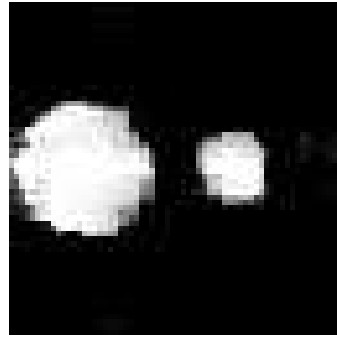
separates the projections of each factor structures, then, in the second step, an EDT method reconstructs the 3D structures.

We have observed that the reconstructed structure of liver and spleen was considerably less smooth than the other factors. The source of the error can be that a part of the large asymmetric volume of the liver partially invisible from certain directions due to the absorption (see, for example, the projection left in Fig. 2). Similar explanation of attenuation can be given in the cases of renal pelvises and bladder (see Table 2).

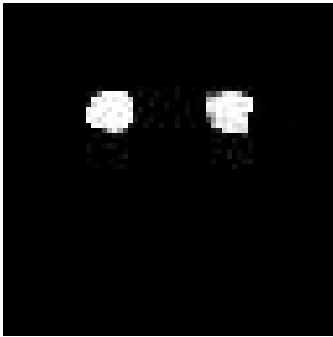
We can conclude that the reconstructed volumes of the factor structures are not far from the right values. Table 2 shows also that our reconstruction



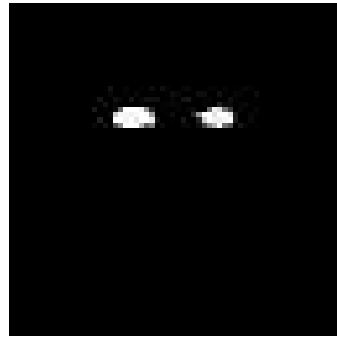
(a) Heart and aorta, Slice 2



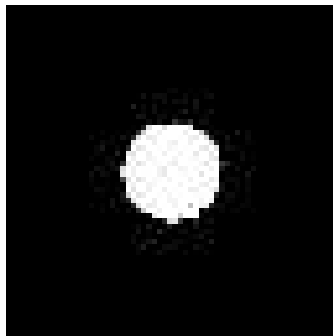
(b) Liver and spleen, Slice 19



(c) Renal parenchyma, Slice 30



(d) Renal pelvis, Slice 39



(e) Bladder, Slice 61

Fig. 7. Images showing the average of the representative reconstructed slices. Darker pixels represents less number of pixels of the corresponding 100 reconstructed structures.

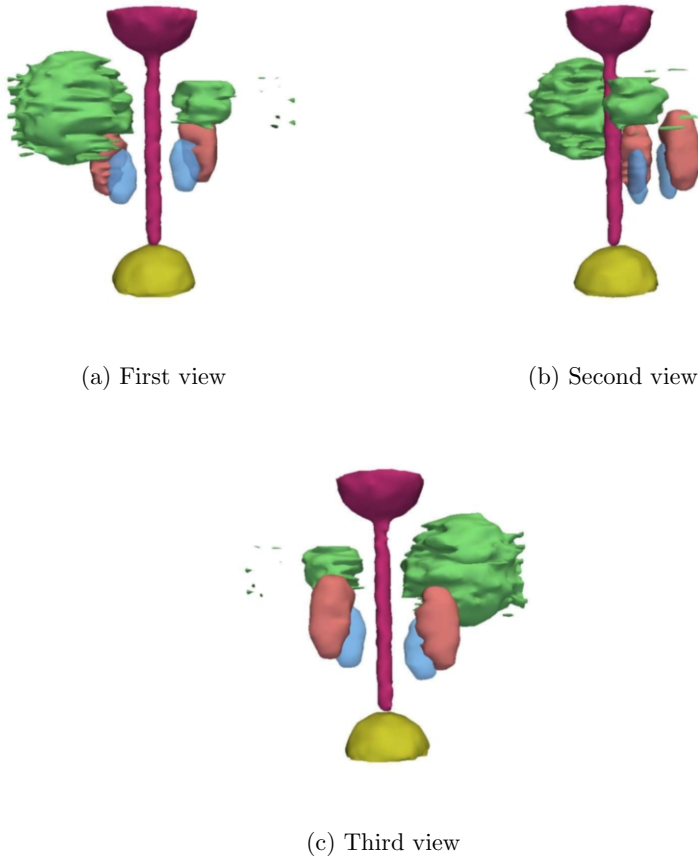


Fig. 8. 3D visualization of the average reconstructed structures.

method is stable.

During the reconstruction we took into account the absorption in the computation of the projections, but we did not make any correction of the scattering and noise. We think that a scatter correction method combined with this procedure would give even better results.

Another point where the procedure can be improved is the determination of the multiplicative constants. Here we plan two modifications: The problem will be simpler if the factor analysis will be performed only on one image sequence (instead of the four sequences of the projections) where each image is the composition of the four corresponding projections. In this way only one

multiplicative constant is to be determined (instead of the four constants used up to now). Another possibility for the determination of the multiplicative constant is if we use the consistency condition derived for absorbed projections [2] recently.

References

- [1] Backfrieder, W., M. Samal, and H. Bergmann, *Towards estimation of compartment volumes and radionuclide concentrations in dynamic spect using factor analysis and limited number of projections*, *Physica Medica* **15** (1999), 160.
- [2] Kuba, A., *Reconstruction of measurable sets from two absorbed projections*, *Technical Report of Dept. of Computer Science*, Univ. of Szeged, 2005.
- [3] Kuba, A. and M. Nivat, *Reconstruction of discrete sets from absorbed projections*, in: G. Borgefors, I. Nyström and G. Sanniti di Baja, editors, *Discrete Geometry for Computer Imagery, Proceedings of the 9th International Conference*, Lecture Notes in Computer Sciences **1953** (2000), 137–148.
- [4] Metropolis, N., A. Rosenbluth, A. T. M. Rosenbluth and E. Teller, *Equation of state calculation by fast computing machines*, *J. Chem. Phys.* **21** (1953), 1087–1092.
- [5] Nagy A. and A. Kuba, *Reconstruction* , to be published in *Acta Cybernetica*.
- [6] Samal, M., M. Karny, H. Surova, E. Marikova, and Z. Dienstbier, *Rotation to simple structure in factor analysis of dynamic radionuclide studies*, *Phys. Med. Biol.* **32** (1987), 371–382.
- [7] Samal, M., C. C. Nimmon, K. E. Britton, and H. Bergmann, *Relative renal uptake and transit time measurements using functional factor images and fuzzy regions of interest*, *Eur. J. Nucl. Med.* **25** (1998), 48–54.
- [8] <http://www.slicer.org>.